Journal of Magnetism and Magnetic Materials 471 (2019) 1–7

Contents lists available at ScienceDirect

Journal of Magnetism and Magnetic Materials

journal homepage: www.elsevier.com/locate/jmmm

Research articles

Long-term stable measurement phantoms for magnetic particle imaging

Lucas Wöckel[a], James Wells[b], Olaf Kosch[b], Stefan Lyer[c], Christoph Alexiou[c], Cordula Grüttner[d], Frank Wiekhorst[b], Silvio Dutz[a,*]

[a] Institut für Biomedizinische Technik und Informatik, Technische Universität Ilmenau, Germany
[b] Physikalisch-Technische Bundesanstalt, Berlin, Germany
[c] Department of Otorhinolaryngology, Head and Neck Surgery, Section for Experimental Oncology & Nanomedicine (SEON), University Hospital, Erlangen, Germany
[d] Micromod Partikeltechnologie GmbH, Rostock, Germany

ARTICLE INFO

Keywords:
Magnetic particle imaging
Magnetic particle spectroscopy
Magnetic nanoparticles
Measurement phantoms

ABSTRACT

Magnetic particle imaging (MPI) is a tomographic imaging method to determine the spatial distribution of magnetic nanoparticles (MNP) within a defined volume. To evaluate the imaging capabilities of existing MPI scanners, their sensitivity and image resolution limits have to be analyzed. Therefore, precisely defined structures (phantoms) with various tracer concentrations are required to enable comparative studies between existing MPI systems. To support the development of capable MPI phantoms, we developed a method to incorporate different commercially available MNP into a long-term stable synthetic polymer with an iron concentration of up to 200 mmol/l. The properties of each type of polymer matrix embedded MNP were tested by magnetic particle spectroscopy (MPS). For shaping the particle loaded polymer to a phantom, we used 3-D printed molds with a structure cross section of $2 \times 2\,mm^2$. The particle loads within the phantoms were then imaged using MPI. The particle-loaded polymer is very suitable for preparation of measurement phantoms that could be visualized by MPI. Repeated shore hardness and MPS measurements up to one year did not reveal any changes in the mechanical and magnetic properties of the used material. In conclusion, we developed long-term stable measurement phantoms for magnetic particle imaging. Further work will focus on more detailed particle loaded structures in phantoms and water based polymers with a more homogeneous particle distribution.

1. Introduction

Magnetic Particle Imaging (MPI) is a rapidly developing imaging technique with high potential for clinical applications [1–3]. This technique detects the response of superparamagnetic nanoparticles (MNP) towards an oscillating external magnetic field. Besides two commercially available MPI systems (Bruker MPI 25/20 FF and Magnetic Insight MOMENTUM imager), the majority of the MPI systems currently running are prototypes, acquiring 1D, 2D, or 3D images. These prototypes essentially differ by coil geometries, voxel size, and strength of the gradient field and used technique to generate field-free regions within the field of view (FOV). Theoretically, these scanners are capable to detect nanomolar concentrations of MNP with a spatial resolution of $1\,mm^3$ [4]. So far, the sensitivity of these scanners is in micromolar range of MNP and a spatial resolution of $1–2\,mm^3$ has been demonstrated experimentally [5,6].

Until now, phantoms for assessment of the imaging performance (sensitivity, temporal and spatial resolution) that can be used in all scanners are not available. To be able to compare precisely these properties, phantoms containing well-defined magnetic structures are required to enable comparative studies between different MPI systems and established clinical imaging techniques. Presently, each lab develops individual measurement phantoms for their MPI measurements. Mostly, phantoms for MPI base on stock or diluted nanoparticle dispersions (liquid phantoms) filled into defined containers or structures. The geometry of the reservoirs for the particle dispersions often is simple and confined to cylindrical shapes arranged in spirals, letters or replicas of arteries [7–10]. In addition to the liquid MNP distributions, there also exist phantoms containing immobilized MNPs. The geometry of the solid state phantoms is mostly engineered by molding or mechanical processing [11,12].

Liquid MNP phantoms have the disadvantage that they are not long-term stable due to decomposition of the core-shell structure, agglomeration, sedimentation, drying of the fluids, or interaction of particles with the container walls. Therefore, such phantoms are not suitable for comparative studies. Furthermore, it has been shown that MNP become

* Corresponding author at: Technische Universität Ilmenau, Institut für Biomedizinische Technik und Informatik, Gustav-Kirchhoff-Straße 2, 98693 Ilmenau, Germany.
E-mail address: silvio.dutz@tu-ilmenau.de (S. Dutz).

https://doi.org/10.1016/j.jmmm.2018.09.012
Received 22 June 2018; Received in revised form 30 August 2018; Accepted 4 September 2018
Available online 10 September 2018
0304-8853/

immobilized immediately after (in-vivo) administration [13,14]. In this case, the resulting behavior of the MPI tracer cannot be emulated correctly by liquid matrix materials. To cope with these problems, we focused on the development of phantom material capable for comparative MPI studies. These should have a defined concentration of MNP and be homogeneously distributed in a solid matrix. Furthermore, the particle-loaded matrix should retain their magnetic and mechanical properties over a long period up to years.

To develop such phantoms, we chosen a synthetic polymer based matrix material and developed a method to embed different types of aqueous MNP in the inorganic polymer via a solvent transfer. The exact shape of the particle-loaded polymer is specified by defined molds. The molds were manufactured by using 3D-CAD software, which guarantees the accuracy of each structure in the following 3D-FFF print. To characterize the mechanical and magnetic properties of our MNP phantoms, we investigated the shore hardness of the phantom materials and performed MPS and MPI measurements.

2. Methods

In previous investigations [15], the synthetic polymer elastosil RT604 (Wacker Chemie AG, München, Germany) showed promising behaviour for the setup of long-term stable phantoms and thus was chosen here as matrix material. This water-insoluble, unvulcanized RTV-2 silicone (silicon and oxygen form the siloxane framework) cure at a temperature of 20 °C. The vulcanization of the polymer is initiated by mixing component A (polymer) and component B (crosslinker) in a ratio of 9:1. The crosslinking temperature should be in the range of 10–200 °C.

Since all MNP types investigated are manufactured in aqueous suspension, and therefore not directly soluble in the elastosil polymer, suitable solvents for the transfer of the MNP from the aqueous phase of the fluid to the organic phase of the elastosil have to be found. We first sought for suitable solvents for dilution of the elastosil without changing the mechanical properties of the matrix. To this end, polyethylene glycol 300 (PEG), acetone, ethanol, propanol, and hexane (all purchased from Carl Roth, Karlsruhe, Germany) were added to 10 ml elastosil in proportions of 0, 5, 10, 15, 20, 25, and 30% by volume and casted in truncated cone shaped test bodies (R_1 = 28.5 mm, R_2 = 26 mm, H = 17.5 mm). These 35 test bodies were degassed in a vacuum chamber at 0.6 bar for three minutes and tempered at 30 °C for one week for curing. After that, the test bodies of this serial dilution were analysed for the occurrence of smudges or bubbles by a stereo microscope (Stemi-2000-C, Zeiss AG, Oberkochen, Germany). To determine the solvent evaporation time from the matrix, the test bodies were weighed repeatedly: immediately after preparation, after 7 days, 14 days, and one year. To investigate the influence of the solvent on the mechanical properties of the matrix, the shore hardness (Shore A) was measured by means of a Shore-A Durometer (Vogel GmbH, Kevelaer, Germany) repeatedly at the same time points.

In the next step we tested, if aqueous MNP types can be transferred into the five different solvents without the formation of agglomerates. For this, we selected four commercially available MNP types, commonly used in MNP research and with promising MPI performance, together with a sample of the SEON group in Erlangen

- perimag® (micromod Partikeltechnologie, Rostock, Germany), c (MNP) = 25 mg/ml
- FeraSpin-R (nanoPET-Pharma, Berlin, Germany), c (MNP) = 100 mg/ml
- fluidMag-D 50 (chemicell, Berlin, Germany), c(MNP) = 100 mg/ml
- Ferucarbotran (Meito Sangyo, Nagoya, Japan), c(MNP) = 200 mg/ml
- $SEON^{LA\text{-}BSA}$ (SEON group, Erlangen, Germany), c(MNP) = 7.8 mg/ml

and mixed 0.5 ml of these samples (diluted with water to a concentration of 5 mg/ml) with 1.5 ml of the solvents and washed it magnetically 3 times with the solvents. After that procedure, the samples of MNP dispersed in the solvents were investigated regarding agglomeration and sedimentation stability.

Since in these investigations ethanol was found to be the only solvent suitable for transfer of MNP into elastosil (see results section), only ethanol was used for the further experiments on the embedding of MNP into elastosil. For this, the MNP stock solutions were magnetically washed three times with ethanol and finally re-suspended in ethanol with an iron concentration of 400 mmol/l, which is a concentration of approximately 22 mg(Fe)/ml. For all five MNP types, elastosil test bodies with embedded MNP were prepared by adding 0.5 ml of the MNP/Ethanol suspension (iron concentrations adjusted to 100, 200, or 400 mmol/l) to 9.5 ml of the polymer. By this way we manufactured different test bodies with an iron concentration c(Fe) adjusted to 5, 10 and 20 mmol/l, respectively. By means of a stereo microscope we investigated, if this procedure leads to the formation of agglomerates within the elastosil matrix. The magnetic performance of the embedded MNP for application in MPI was characterized by means of Magnetic Particle Spectroscopy (MPS). For this, samples of the aqueous MNP fluids as well as the MNP embedded into the elastosil were investigated. MPS measurements were conducted using a commercial and calibrated MPS system (MPS-3, Bruker, Germany) operating at a fixed excitation frequency of 25.25 kHz with an adjustable amplitude ranging from 0 to 25 mT. Signals were detected using a gradiometric pick-up coil with an inner diameter of 12 mm. For all measurements in this study, an excitation amplitude of 25 mT and a total acquisition time of 10 s were chosen. Measurements of empty sample holders were subtracted from the raw sample data to remove time-constant background components contained in the signal. The device internally performs a Fourier transformation of the detected time domain signals and outputs all frequency components in units of Am^2 (internal calibration procedure using a calibrated coil).

To prepare measurement phantoms, first, molds with notches for the imaging structures, which has to be filled up with MNP, were designed,

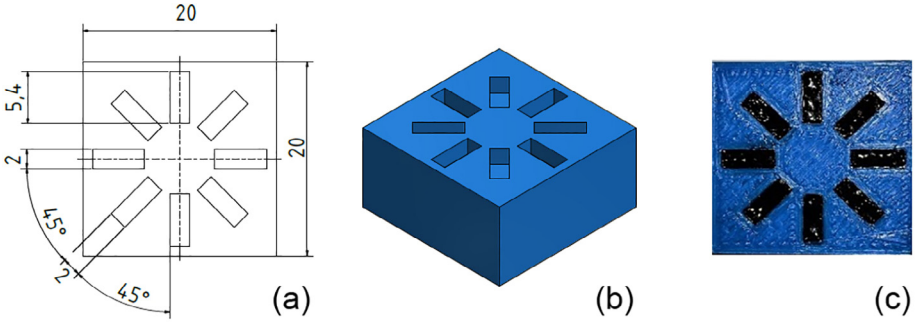

Fig. 1. (a) Sketch and (b) 3D-CAD model of the mold and (c) printed mold with MNP-loaded-polymer filled structures.

see Fig. 1. The molds were printed on a 3D printer (Raise3D N2 Plus, Raise3D INC., Costa Mesa, USA) by using filaments of polylactide (filamentworld, Neu-Ulm, Germany) with an outer diameter of 1.75 mm. The printing parameters were adapted to the specifications of the filament manufacturer (printing speed: 70 mm/s, nozzle temperature: 200 °C, heat bed temperature 60 °C).

Second, three molds were filled with perimag® (15 µL volume per notch, 120 µL in total), in a fluid state, and freeze-dried in a sugar matrix (mannitol) at c(Fe) = 152 mmol/L, as well as perimag® embedded in elastosil at c(Fe) = 200 mmol/L. Then, each phantom was imaged by MPI using a preclinical MPI scanner (Bruker MPI 25/20 FF) installed at Charité University Hospital Berlin, equipped with an additional separate receiving coil [16] to increase sensitivity. This device is a field-free-point (FFP) scanner where the FFP is moved on a 3D Lissajous-trajectory generated by three orthogonal magnetic drive fields (DF) of 12 mT amplitude oscillating at slightly different frequencies (about 25 kHz). Spatial encoding is achieved by applying static magnetic gradient fields ($G_x = G_y = 1.25$ T/m, $G_z = 2.5$ T/m). The image reconstruction is based on the system function (SF) approach for MPI, where a point-like MNP sample is used for calibration. Three SFs were measured using three different perimag® samples (fluid, freeze-dried in a mannitol matrix, and embedded in elastosil) of 13.5 µL filled into a rectangular sample container (3·3·1.5 mm^3). The SFs are acquired over a rectangular volume of 26.4·26.4·13.2 mm^3 sampled on a grid of 33·33·33 voxel (resulting in a voxel size of 0.8·0.8·0.4 mm^3). MPI measurements of the phantoms were performed using the same field parameter as for SF acquisition. First, the background signal was recorded without the phantom, followed by the measurement with the phantom at the FOV center. Then, the background was subtracted from the recorded data and frequency components with a SNR > 5 selected for image reconstruction using the Kaczmarz algorithm with 20 iterations and a regularization factor of 10^{-5}.

3. Results and discussion

The optical investigation of the dilution series test bodies revealed, that hexane is the most suitable solvent for the dilution of elastosil, see Fig. 2. For all concentrations (0 to 30% by volume) no smudges or bubbles were observed in the test bodies. Dilution by ethanol led to the formation of bubbles for concentrations of 20% and above. Similar results were obtained for Isopropanol for concentration of ≥15% and Acetone for ≥10%. For PEG a strong blurring of the elastosil was observed for all concentrations.

Resulting from these observations it can be concluded that, hexane, ethanol, and isopropanol are the most promising solvents for the dilution of elastosil by up to 10% by volume relating to occurrence of bubbles within the elastosil.

The weight measurement of the diluted elastosil test bodies during curing and after one-year storage clearly demonstrate, that the solvents hexane, ethanol, isopropyl alcohol and acetone vaporized completely from the polymer within the first seven days after preparation because the weight after seven days differs only slightly from the reference sample (0 vol.-% solvent in polymer), see Fig. 3a/c. Also in following measurements (after 14 days and one year) no significant alterations in weight were observed. The weight measurements of the test bodies with PEG indicate a large proportion of PEG remaining in the elastosil after seven and 14 days, see Fig. 3e. After one year, a slight weight loss compared to the measurements after seven and 14 days can be observed. Since PEG-300 cannot evaporate at temperatures tolerable for elastosil due to its physico-chemical properties, it remains in the polymer. For this investigation it can be concluded that all tested solvents except the PEG evaporate from the polymer after a short time and thus are suitable for solvent transfer of MNP into elastosil.

The shore hardness of the hexane samples is close to the reference hardness of 23 shore A for dilutions up to 10%. For stronger dilutions, a moderate decrease of the shore hardness results. The ethanol samples have a constant shore A hardness of 23 up to a solvent concentration of 15%, which did not change over one year, see Fig. 3b. For higher dilutions, a remarkable decrease of the hardness can be observed. The dilution of elastosil by acetone, isopropyl alcohol, and PEG-300 leads to significant decrease of the shore hardness of the polymer for all tested solvent concentrations.

The results of the shore-A measurement show significant differences in hardness between the solvent-polymer test bodies. For some concentrations, in isopropanol, ethanol, and acetone samples gas bubbles are visible (see Fig. 2). The inclusion of the gas explains the reduced Shore hardness of higher concentrated solvent-polymer samples, because the gas inclusions are compressible and change the viscoelastic properties of the polymer. For this reason, it can be said that increasing the gas inclusions in the samples results in a lower Shore A value. Furthermore, it can be observed, that shore hardness for seven or 14 days show significant deviations and a hardening occurs between seven and 14 days. Taking into account that the solvents hexane, ethanol, isopropyl alcohol, and acetone are evaporated from the polymer as shown before within 7 days, there must be a second effect which influences the crosslinking of the polymer.

For the investigation of the transfer of aqueous MNP into the different solvents it was found, that all MNP samples are completely dispersable in ethanol, isopropanol, and PEG whereas a strong agglomeration and sedimentation was observed for all MNP samples in combination with acetone and hexane.

Resulting from all the findings described above, only ethanol seemed to be a suitable solvent for the transfer of the aqueous MNP into elastosil without any influence on the mechanical properties of the elastosil matrix and the agglomeration state and solubility of the aqueous MNP fluids. Therefore, for the next experiments regarding embedding of different MNP into elastosil only ethanol was used for the solvent transfer. The visual characterisation of the MNP loaded test bodies revealed a uniform coloring of the polymer for all different MNP. Investigation of the test bodies by means of a microscope showed, that Ferucarbotran, $SEON^{LA\text{-}BSA}$, and perimag® particles are well dispersed in the elastosil matrix. For Feraspin and fluidmag large MNP agglomerates of several µm were present within the test bodies.

We investigated the influence of embedding the MNP in elastosil on the magnetic properties by MPS measurements of the corresponding samples together with fluid and immobilized MNP samples as references. Fig. 4a shows MPS spectra (odd harmonics normalized to the sample iron amount) of perimag® and $SEON^{LA\text{-}BSA}$ reference samples (liquid and immobilized). Obviously, samples in the liquid state exhibit higher amplitudes than after immobilisation. Furthermore, the normalized spectrum of perimag® is higher than that of $SEON^{LA\text{-}BSA}$. Feraspin and Ferucarbotran exhibit amplitudes in the range of perimag®, while the amplitude of fluidmag is more in the range of $SEON^{LA\text{-}BSA}$. The corresponding characteristic parameters are summarized in

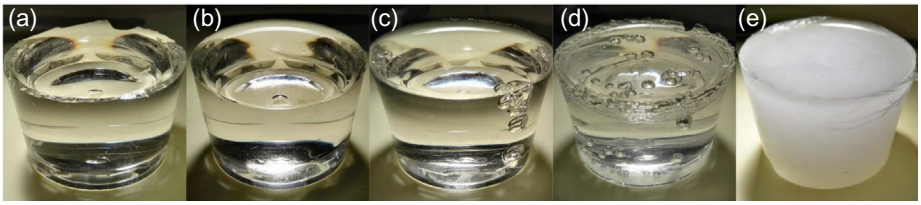

Fig. 2. Photographs of the test bodies consisting of elastosil diluted by 15% by volume of (a) hexane, (b) ethanol, (c) isopropanol, (d) acetone, and (e) PEG-300. Please note that the bubble on the bottom of each test body is an artefact due to the casting procedure of the test body.

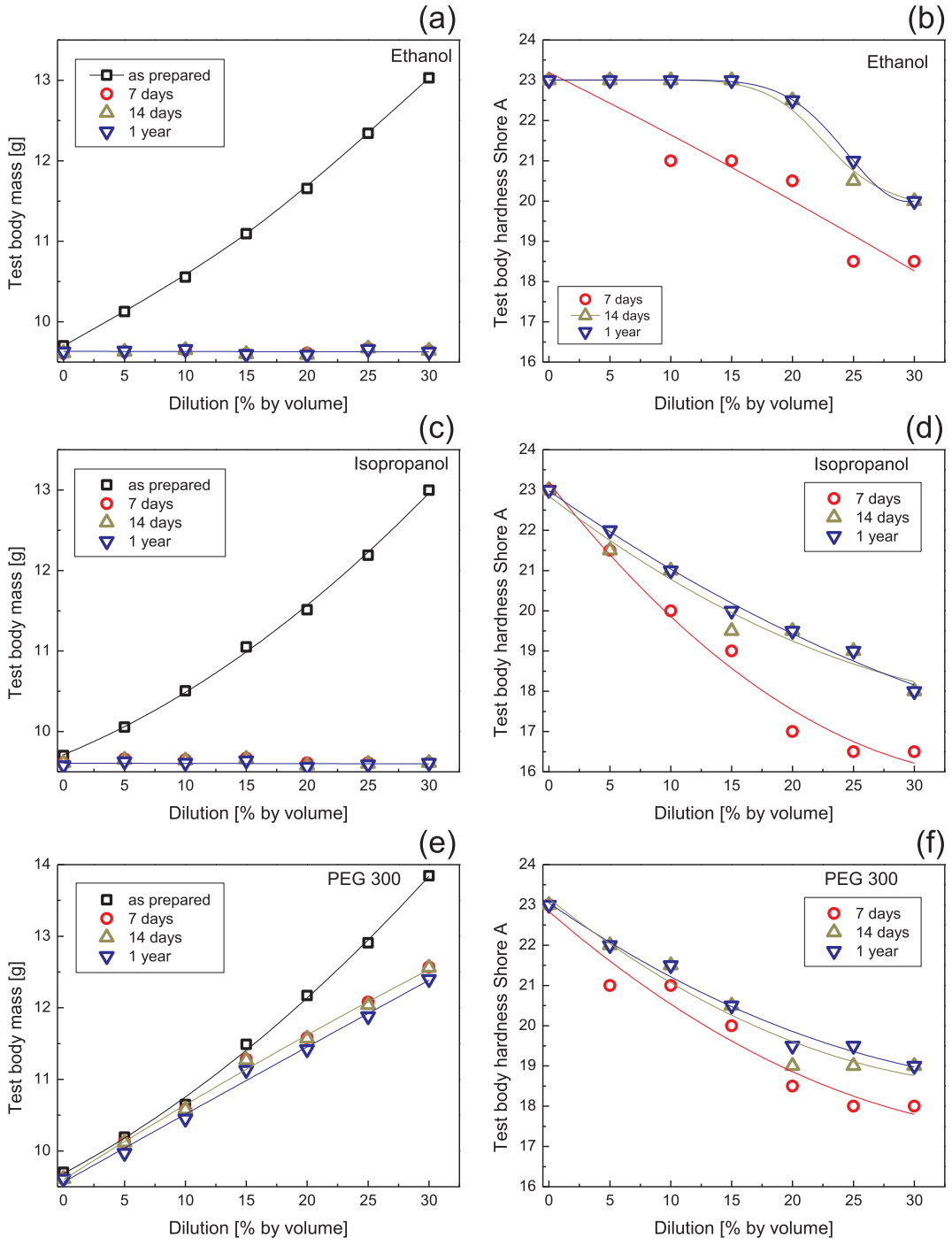

Fig. 3. Mass (left) and Shore-A hardness (right) of the test bodies for several time points after preparation for the solvents (a, b) ethanol, (c, d) isopropanol and (e, f) PEG-300; lines serve only as a guide to the eye.

Table 1.

A loss of MPS signal amplitude after immobilisation is commonly observed for all MNP types and is attributed to the elimination of Brownian rotation reducing the dynamic magnetic response of the MNP. As summarized in Table 1, this behaviour is confirmed for all MNP samples investigated, as well. Additionally, we observe in all systems embedded in elastosil a stronger drop in A_3^* as in immobilized samples of the same system. We attribute this to the observed strong aggregation tendency of the MNP due to the ethanol treatment prior to elastosil embedding. This aggregation can only partly be dispersed and decreases the dynamic magnetic response of the MNP due to particle-particle interactions.

Though there is a pronounced MPS amplitude loss for all systems, there is a distinct behaviour in the shape of the spectra (important for MPI image quality) as expressed by the ratio of fifth to third harmonic A_5/A_3 which is independent on the amount of MNP in a sample. Here, some MNP systems like perimag®, FeraSpin-R, and Ferucarbotran show a steep decrease of A_5/A_3 after embedding in elastosil, while the systems SEON$^{\text{LA-BSA}}$ and fluidMag-D 50 maintain nearly the same A_5/A_3 value irrespective their state.

The temporal stability of the dynamic magnetic behaviour of the elastosil phantoms is exemplified in Fig. 5, which shows the MPS spectra of perimag® and SEON$^{\text{LA-BSA}}$ embedded in elastosil measured 1 day and remeasured after storage of one year at room temperature at

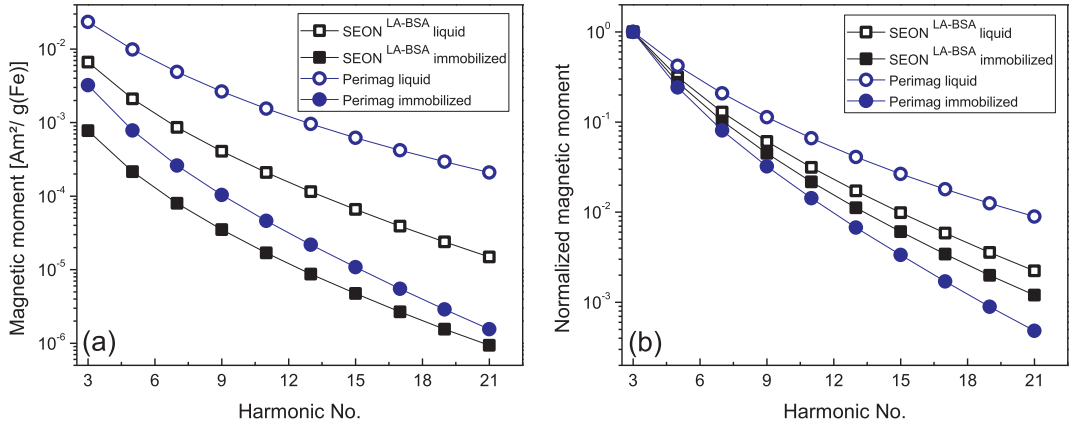

Fig. 4. Effect of immobilization on the dynamic magnetic behaviour of SEON^{LA-BSA} (squares) and perimag® MNP (circles) for liquid (open symbols) and immobilized (close symbols) conditions, (a) MPS amplitudes of harmonics A_i normalized to iron amount showing the signal amplitude and (b) normalized to the amplitude A_3 to compare the curve shapes; lines serve only as a guide to the eye.

ambient atmosphere. For perimag®, no significant change in the dynamic behaviour is observed, whereas for SEON^{LA-BSA} a slight decrease in MPS amplitude can be seen. Very probably, due to the high surface-to-volume ratio of these relatively small particles, a stronger oxidation to iron oxides with different magnetic properties or to a non-magnetic dead layer takes place and a stronger decrease of the signal intensity and the spectra of the higher harmonics can be found for the sample after storage for one year compared to the as prepared sample. As can be seen in Table 1, there is a strong decrease (more than 50%) in A_3^* for all samples in the fluid state after storage of one year. This is not surprising since these samples of 10 µL volume were stored in their container in between the measurements at 4 °C, but without any protection against evaporation. Nevertheless, the shape factors A_5/A_3 only show minute changes. Similar there is a drop in A_3^* noticeable for the MNP immobilized (in plaster), even though less pronounced.

The least changes over time show in fact the MNP embedded in elastosil for both characteristic values A_3^* (below 8%, except SEON^{LA-BSA} with 35%) and A_5/A_3 (below 1%). Thus, it seems that elastosil effectively protects the MNP against degradation and oxidation. Fig. 6 verifies the temporal stability of the shape factor A_5/A_3 for the MNP systems perimag® and SEON^{LA-BSA} over a period of one year for the different states fluid, immobilized and embedded in elastosil.

Taking into account all results, we chose perimag® embedded in elastosil (after solvent transfer by using of Ethanol) as the most promising long-term stable material combination and finally, prepared

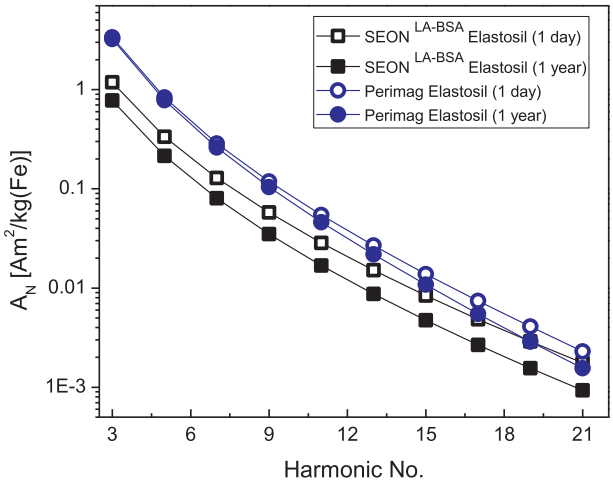

Fig. 5. Dynamic magnetic behaviour of perimag® (circles) and SEON^{LA-BSA} (squares) embedded in elastosil. MPS spectra measured at 25 mT normalized to iron amount measured 1 day after preparation (open symbols) and the same samples remeasured after storage of one year (full symbols); lines serve only as a guide to the eye.

Table 1
Characteristic parameters of the five MNP systems investigated. Particle (mean) core diameter D_c and hydrodynamic diameter D_h, the state (fluid, immobilized, after ethanol transfer, embedded in elastosil), specific MPS amplitude A_3^* and shape factor A_5/A_3 after 1 day, 1 year storage, and relative change.

Sample	Particle size [nm]		Immobilization	A3* [Am²/kg(Fe)]			A5/A3 [%]		
	D_c	D_h		1 day	1 year	ΔA3*	1 day	1 year	ΔA5/A3
perimag®	3–8	106	Fluid	18.31	10.50	42.7%	42.71	42.09	0.62
			Immobilized	13.10	10.50	19.8%	39.37	36.62	2.75
			Ethanol	9.58			32.44	–	–
			Elastosil	3.36	3.23	4.1%	24.72	24.19	0.53
SEON^{LA-BSA}	11	62	Fluid	8.44	1.96	76.8%	31.88	31.54	0.34
			Immobilized	7.76	6.06	22.0%	31.09	28.45	2.64
			Elastosil	1.18	0.78	34.2%	28.29	27.55	0.74
FeraSpin™-R	5–8	60	Fluid	8.62	5.13	40.5%	40.78	40.30	0.48
			Immobilized	5.87	2.33	60.3%	34.42	33.30	1.12
			Elastosil	2.85	2.71	4.9%	27.09	27.03	0.06
Ferucarbotran	4–9	45–60	Fluid	8.43	2.39	71.7%	41.72	40.62	1.10
			Immobilized	7.86	5.32	32.3%	40.66	34.55	6.11
			Elastosil	3.21	2.98	7.0%	28.94	27.96	0.98
fluidMag-D 50	6	50	Fluid	5.87	1.55	73.6%	31.32	30.15	1.17
			Immobilized	5.88	5.19	11.8%	30.29	30.26	0.03
			Elastosil	3.75	3.68	1.8%	27.20	27.25	0.05

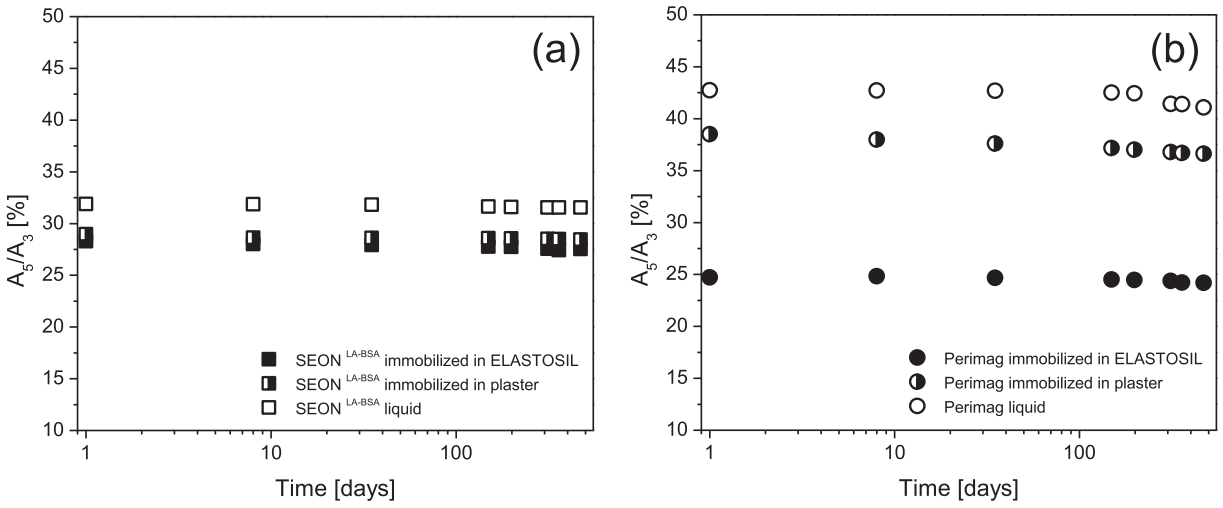

Fig. 6. Long-term dynamic magnetic behaviour of (a) SEON^{LA-BSA} (squares) and (b) perimag® (circles) MNP immobilized within plaster as well as elastosil, A5/A3 ratio as function of storage time.

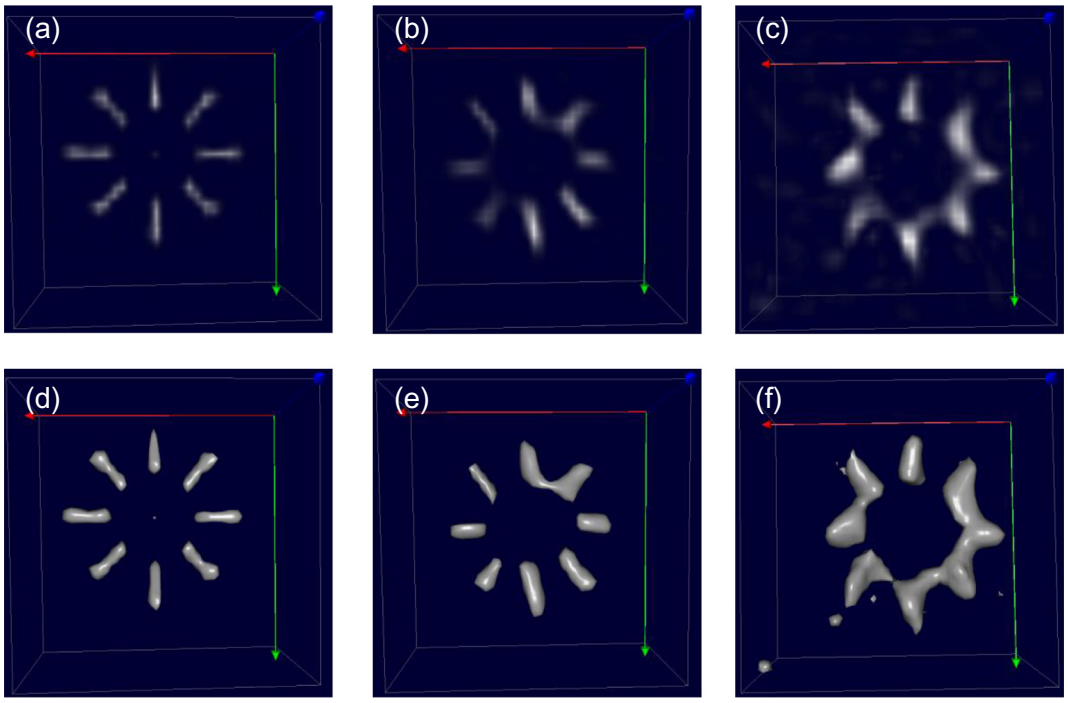

Fig. 7. Reconstructed MPI mages of the phantom. The structures are filled with perimag®: (a, d) liquid, (b, e) freeze dried in mannitol, and (c, f) dispersed in elastosil. Shown are (a-c) intensity value images of the particle distribution and (d-f) the volume image Iso3.

measurement phantoms for MPI.

For imaging investigations, the structures of the phantoms were filled with perimag® (liquid, immobilized in mannitol, or dispersed in elastosil) and imaged by MPI. Fig. 7 shows the intensity value images of the particle distribution as well as the volume image (Iso3), where the volume includes all regions of the distribution where the intensity is not lower than 30% of the maximum intensity.

First of all, all three tested mobility states of perimag® can be imaged in MPI. It becomes obviously, that immobilizing the MNP in mannitol and elastosil leads to a decrease of the spatial resolution of the reconstructed images. As discussed before, this is due to the loss of signal amplitude and decreasing ratio of higher harmonics, which finally leads to a reduced dynamic response of the MNP after immobilization. Nevertheless, taking into account the small dimensions of MNP loaded structures within the phantom, it can be confirmed from the imaging investigations, that the combination of perimag® in elastosil is a suitable tracer material for the preparation of long-term stable measurement phantoms which can be imaged in MPI.

4. Conclusion

In this study, long-term stable materials for the preparation of measurement phantoms for magnetic particle imaging were established. For this, a route for the embedding of aqueous MNP into an inorganic polymer (elastosil) on the base of a solvent transfer of the particles by using ethanol is demonstrated. The magnetic performance of the MNP during all different preparation steps of the phantoms was recorded by means of MPS. A decrease of tracer performance was found especially after the transfer to ethanol and after embedding into elastosil. Due to the good signal intensity of the used perimag® MNP and

the excellent long-term stability after embedding the MNP into elastosil, this disadvantage could be accepted on the way to the preparation of long-term stable measurement phantoms.

Finally, we could demonstrate, that the combination of perimag® dispersed in elastosil is a suitable material for the preparation of long-term stable measurement phantoms for MPI. The material shows a good MPS signal which is long-term stable of at least one year and during this time interval also the mechanical properties of the matrix doesn't change.

In ongoing work we focus on the use of a water based polymer matrix for embedding the particles without a solvent transfer step, aiming on an improvement of tracer performance for long-term stable embedded MNP.

Acknowledgements

This work was supported by Deutsche Forschungsgemeinschaft (FKZ: DU1293/6-1, TR408/9-1, and AL552/8-1), the German Federal Ministry of Education and Research (BMBF) as part of the InnoProfile project "MAMUD" (03IPT605X), and the Emerging Fields Initiative (BIG-THERA).

References

[1] B. Gleich, R. Weizenecker, Tomographic imaging using the nonlinear response of magnetic particles, Nature 435 (2005) 1214–1217.
[2] D. Hensley, Z.W. Tay, R. Dhavalikar, B. Zheng, P. Goodwill, C. Rinaldi, S. Conolly, Combining magnetic particle imaging and magnetic fluid hyperthermia in a theranostic platform, Phys. Med. Biol. 62 (2017) 3483.
[3] K. Murase, M. Aoki, N. Banura, K. Nishimoto, A. Mimura, T. Kuboyabu, I. Yabata, Usefulness of magnetic particle imaging for predicting the therapeutic effect of magnetic hyperthermia, Open J. Med. Imaging 5 (2015) 85.
[4] S. Herz, P. Vogel, T. Kampf, M. Rückert, S. Veldhoen, V. Behr, T. Bley, Magnetic particle imaging for quantification of vascular stenoses: a phantom study, IEEE Trans. Med. Imaging 37 (2018) 61–67.
[5] H. Paysen, J. Wells, O. Kosch, U. Steinhoff, L. Trahms, T. Schaeffter, F. Wiekhorst, Towards quantitative magnetic particle imaging: a comparison with magnetic particle spectroscopy, AIP Adv. 8 (2018) 056712.
[6] T. Viereck, C. Kuhlmann, S. Draack, M. Schilling, F. Ludwig, Dual-frequency magnetic particle imaging of the Brownian particle contribution, J. Magn. Magn. Mater. 427 (2017) 156–161.
[7] R.M. Ferguson, A.P. Khandhar, S.J. Kemp, H. Arami, E.U. Saritas, L.R. Croft, J. Konkle, P.W. Goodwill, A. Halkola, J. Rahmer, Magnetic particle imaging with tailored iron oxide nanoparticle tracers, IEEE Trans. Med. Imaging 34 (2015) 1077–1084.
[8] K. Gräfe, G. Bringout, M. Graeser, T.F. Sattel, T.M. Buzug, System matrix recording and phantom measurements with a single-sided magnetic particle imaging device, IEEE Trans. Magn. 51 (2015) 1–3.
[9] J.J. Konkle, P.W. Goodwill, D.W. Hensley, R.D. Orendorff, M. Lustig, S.M. Conolly, A convex formulation for magnetic particle imaging X-space reconstruction, PloS One 10 (2015) e0140137.
[10] S. Vaalma, J. Rahmer, N. Panagiotopoulos, R.L. Duschka, J. Borgert, J. Barkhausen, F.M. Vogt, J. Haegele, Magnetic particle imaging (MPI): experimental quantification of vascular stenosis using stationary stenosis phantoms, PloS One 12 (2017) e0168902.
[11] C. Jacobi, T. Friedrich, K. Lüdtke-Buzug, Synthesis and characterisation of superparamagnetic polylactic acid based polymers, Int. J. Magn. Particle Imaging 3 (2017).
[12] J. Rahmer, H. Rahn, F. Henrich, S. Odenbach, B. Gleich, J. Borgert, Solid state MPI: imaging of iron oxide nanoparticles embedded in polyurethane, Magnetic Particle Imaging (IWMPI), 2013 International Workshop on, IEEE, (2013) pp. 1–1.
[13] S. Dutz, M. Kettering, I. Hilger, R. Muller, M. Zeisberger, Magnetic multicore nanoparticles for hyperthermia-influence of particle immobilization in tumour tissue on magnetic properties, Nanotechnology 22 (2011) 265102.
[14] H. Richter, M. Kettering, F. Wiekhorst, U. Steinhoff, I. Hilger, L. Trahms, Magnetorelaxometry for localization and quantification of magnetic nanoparticles for thermal ablation studies, Phys. Med. Biol. 55 (2010) 623–633.
[15] L. Wöckel, Herstellung langzeitstabiler Messobjekte für die Magnetpartikelbildgebung auf Basis etablierter Tracerpartikel in einer Silikonmatrix, Technische Universität Ilmenau (2017).
[16] J. Wells, H. Paysen, O. Kosch, N. Löwa, F. Schmitzberger, M. Makowksi, J. Franke, L. Trahms, F. Wiekhorst, Characterizing a preclinical magnetic particle imaging system with separate pickup coil, IEEE Trans. Magn. 53 (2017) 1–5.